Contents lists available at SCCE

Journal of Soft Computing in Civil Engineering

Journal homepage: www.jsoftcivil.com

Assessment of Micro-pile Group Capacity in Soft Clay Soils Using Closed-Form Machine Learning Models

Tammineni Gnananandarao [1,*]; Naga Dheeraj Kumar Reddy Chukka [1]; B.A.V. Ram Kumar [2]; Jayatheja Muktinutalapati [3]; Vedprakash Maralapalle [4]; Satish Kumar Mummidivarapu [1]; CH. Ajay [1]; P. Uma Maheswara Rao [1]

1. Department of Civil Engineering, Aditya University, Surampalem, Andhra Pradesh, India, 533437
2. Department of Civil Engineering, GMR Institute of technology, Rajam, Andhra Pradesh, India
3. RICS School of Built Environment, Amity University Maharashtra, Mumbai, 410206, India
4. Associate Professor, L. S. Raheja School of Architecture, Bandra, Mumbai, 400051, India

* Corresponding author: *gnananandarao.tammineni@acet.ac.in*

https://doi.org/10.22115/scce.2025.501243.2023

ARTICLE INFO

Article history:
Received: 24 January 2025
Revised: 22 May 2025
Accepted: 14 August 2025

Keywords:
Micro-piles;
Soft clay soil;
Artificial neural networks;
M5P model.

ABSTRACT

The computation of the in-situ load-bearing capacity of micropiles for different soil types using conventional methods is often difficult and time-consuming. Machine learning models, on the other hand, offer promising outcomes by predicting real-time solutions without requiring extensive traditional calculations. In this study, models such as Artificial Neural Networks (ANN) and the M5P model tree are developed using a dataset of 434 experimental results obtained from previous studies. The accuracy of the ANN model is evaluated using the correlation coefficient (R^2), which was observed to be 0.99 for both training and testing, with mean absolute percentage errors (MAPE) of 18.38 and 7.67, respectively. Similarly, the M5P model tree achieved an R^2 of 0.99, with corresponding MAPE values of 23.92 and 10.01, which were slightly higher than those of the ANN model. The equations developed by both models demonstrated a strong correlation factor with minimal errors. The primary influencing parameters identified were Se/b and n. Although both models performed well, ANN was found to be more effective than the M5P model, as it exhibited lower relative errors and higher accuracy in predictions.

How to cite this article: Gnananandarao T, Chukka NDKR, Muktinutalapati J, Maralapalle V, Kumar BAVR, Ajay CH, Kumar MS, Uma Maheswara Rao P. Assessment of micro-pile group capacity in soft clay soils using closed-form machine learning models. Journal of Soft Computing in Civil Engineering. 2026;10(3):2023. https://doi.org/10.22115/scce.2025.501243.2023

1. Introduction

Micropiles, popularly known as small-diameter piles, have gained global prominence due to their various advantages over conventional piles. They offer high load-bearing capacity in diverse soil types, easy installation with minimal noise and vibration, low settlement rates, and effective performance in low-headroom access areas [1]. The construction process of micro piles involves cement grouting and reinforcing elements, which can be installed without casing, either through gravity or pressurized grouting [2]. Micropiles can be installed directly under footings to transfer the load to the surrounding soils, even in weak soil conditions [1,3]. Furthermore, micropiles are used for retrofitting existing foundations or improving soil stability [1–3].

The application of micropiles in various scenarios, particularly their effectiveness in soft clays, is novel and warrants further exploration. Most coastal areas and northeastern states of India consist of soft clay, characterized by low shear strength, high compressibility, and significant settlement, necessitating the use of micropiles [4]. A proper technical understanding of micropile technology can enhance its adoption as an economical solution to these challenges. However, Micropile implementation in soft clay soils can face challenges such as excessive settlement and reduced load-bearing capacity due to the compressibility and low shear strength of clay. Achieving sufficient skin friction and end-bearing resistance may also be difficult, potentially leading to negative skin friction or downdrag effects. Additionally, ensuring effective grout penetration can be problematic in low-permeability clay, impacting the bond strength between the pile and surrounding soil.

The conventional methods for computing pile load capacity are time-consuming, labour-intensive, and prone to potential errors due to manual calculations. Soft computing models like Artificial Neural Networks (ANN) and M5P, based on previously collected data, can simplify these traditional processes and facilitate the prediction of load-bearing capacity for various foundations and soil conditions. These models are highly effective in accurately identifying nonlinear relationships in geotechnical engineering applications. The current study focuses on determining the vertical load-carrying capacity of micropile groups installed in soft clay using ANN and M5P models.

2. Background

Extensive research has been conducted on the performance of micropiles under vertical compressive loads using both numerical and experimental approaches. Some studies have examined the behavior of micro piles under applied loads, while others have predicted their behavior through computational methods, including data mining [5–8].

In civil engineering applications, the formulation of nonlinear model relationships using Artificial Neural Networks (ANN) has proven to be promising due to its accuracy and feasibility [9,10]. Several studies have addressed geotechnical issues and their corresponding limitations using ANN-based models. The nonlinear relationships were developed to model the shear strength and matric suction in unsaturated soils [11]. Cement stabilized soft soil, compressive strength was estimated [12], while [13] developed models to predict the unconfined compressive strength of fly ash-stabilized organic clay. [14] used ANN to evaluate the erodibility of unsaturated soil treated with quarry dust fines. ANN has also been effective in developing models for estimating the ultimate bearing capacity of layered soils for surface footings [15] . Additional models have been proposed for skirted footings on sand and strip footings subjected to inclined eccentric loading [16]. Furthermore, [17] applied ANN to predict tsunamigenic seismic activity using seismic data, showcasing the versatility of ANN in civil engineering applications.

Similarly, M5P models, which are tree-based structures with regression capabilities, have been effectively used to address various geotechnical problems. Data collected from Haryana state was utilized to determine geotechnical engineering parameters using various machine learning techniques, one of which involved the M5P model. [18] developed an M5P model to estimate the ultimate bearing capacity of cohesionless soil for shallow foundations. Additionally, [19] used the M5P model to predict the impact of industrial waste on the compressive strength of concrete. The bearing capacity of circular footings resting on the confined thickness of sand layers under eccentric-inclined loading conditions was also analyzed using M5P and ANN models, contributing to its effectiveness in such complex scenarios [20]. Other models were developed by Borthakur (SVM Model) and based on experimental and numerical data to find the group capacity of micro piles in clayey soils [21]. Tree-based models have been employed to predict tunnel boring machine performance and classify rock masses in tunnel construction based on rock and material properties [22,23] Additionally, these models have been used to assess the factors influencing the bearing capacity of friction piles [24] and to estimate the powder factor in mine blasting [25]. The statistical summary of previous studies for the ANN and M5P models is presented in Table 1. A review of Table 1 reveals that, both the ANN and M5P models are capable of estimating various civil engineering applications.

Table 1
Statistical Summary of ANN and M5P models.

Model	Application	R^2	r	RMSE	MAE
ANN [9]	Pile load capacity	-	0.985	-	-
ANN [11]	Unsaturated shear strength	0.91	-	-	-
ANN [13]	Unconfined Compressive Strength (UCS) of Fly Ash (FA)Stabilised Organic Clay	0.96	0.994	46.88	32.65
ANN [19]	compressive strength of concrete	0.99	0.99	5	3.77
ANN [20]	Circular Footing Seating on the Limited Thick Sand-Layer with Eccentric Inclined Load	0.99	0.98	39.6	28.98
ANN [9]	Settlement of foundation	-	0.99	3.9	2.6
M5P [13]	UCS of FA Stabilised Organic Clay	0.95	0.976	50.9	39.48
M5P [16]	Ultimate Bearing Capacity of Strip Footing Subjected to Eccentric Inclined Load	0.997	0.998	0.047	0.036
M5P [18]	Ultimate Bearing Capacity of Shallow Foundations on the Cohesionless Soils	0.99	0.97	0.347	0.33
M5P [19]	Compressive strength of concrete	0.99	0.99	4.92	4.05
M5P [20]	Circular Footing Seating on the Limited Thick Sand-Layer with Eccentric Inclined Load	0.99	0.96	47.68	32.13

R^2 = Coefficient of determination, r = Coefficient of correlation, RMSE = root mean square error, MAE = Mean absolute error, '-' = data not available

Based on the above literature review, it can be concluded that there are limited studies on the bearing capacity of micropiles resting on soft clay, particularly with regard to predictions using developed model equations. Hence in this current study focuses on predicting the load-carrying capacity of micropile groups using ANN and M5P models to develop the model equations. Data acquired from previous studies were used to develop these models, and further sensitivity analysis and empirical relationships were derived. These developed models can provide valuable insights for geotechnical practitioners, enabling them to predict the load-bearing capacity of micro-pile groups in soft clays without undergoing the laborious process of conventional computations.

3. Data set

A total of 434 datasets were acquired from previous studies conducted in an excavated pit with dimensions of 2 × 4 × 3 m. The data was randomly divided into two parts: 70% was used for training, and 30% was used for testing. The input parameters included d/b, l/b, n, s/b, h, and s_e/b while q_s/c_u was the output parameter. Here, d represents the micro-pile diameter, b is the size of the micropile cap, l is the micropile length, n is the total number of micropiles in the group, s is the spacing between micropiles, h denotes the position of the micropile cap relative to the ground surface, s_e is the settlement of the pile group, q_s is the load intensity, and c_u is the undrained shear strength of the clay. The total data is shown in the Fig. 1 as in the form of histogram. Fig. 2 presents a heat map of the correlation matrix, offering insights into the relationship coefficients among the input and output variables. Table 2 presents the statistical summary of the data entries in relation to the analyzed parameters.

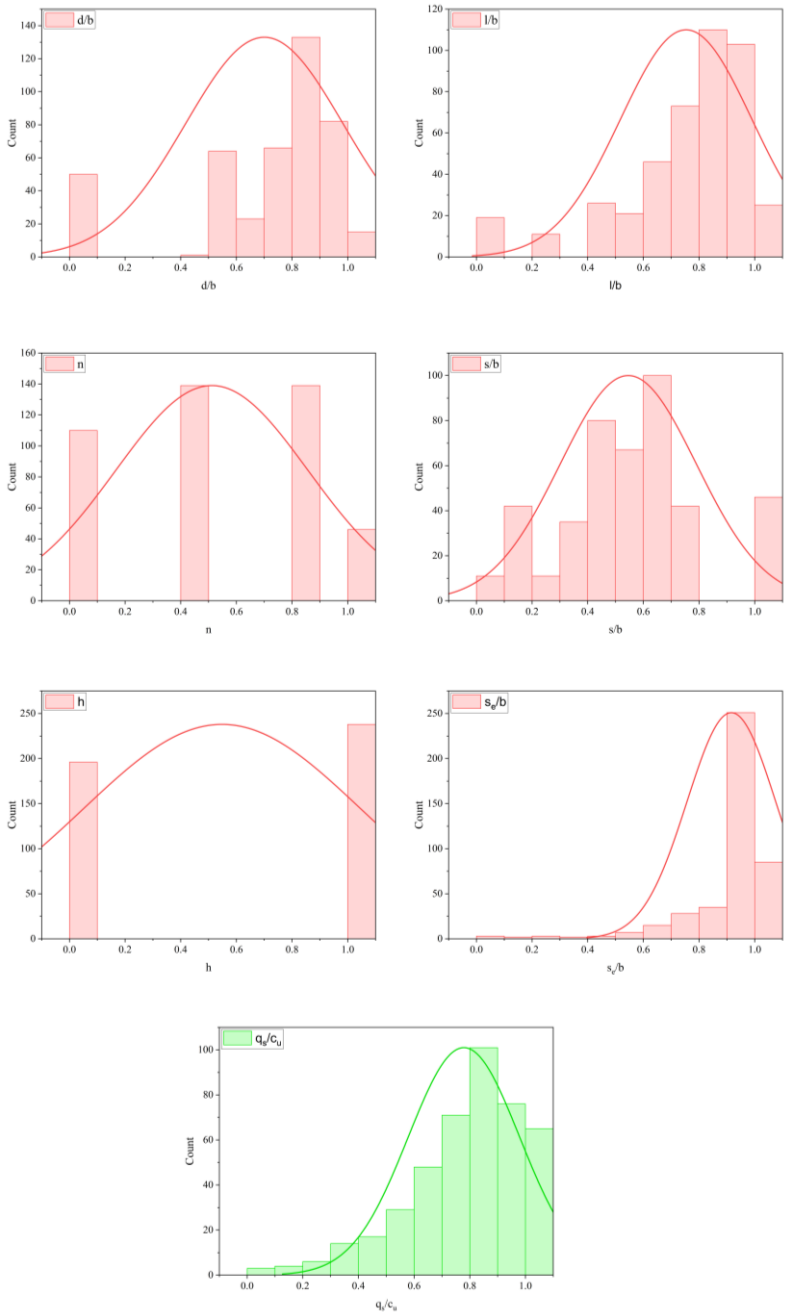

Fig. 1. Histogram for distribution of input parameters and output parameter.

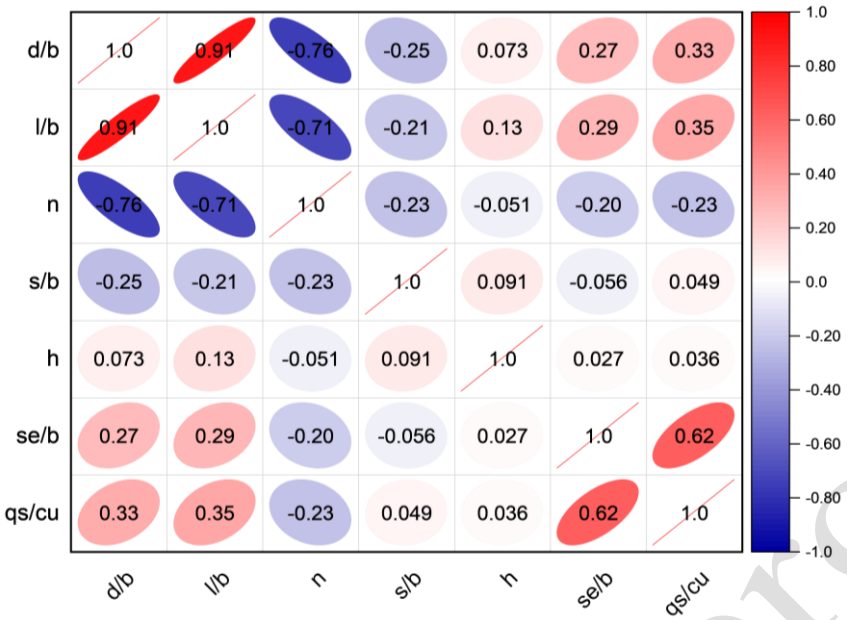

Fig. 2. Pearson's correlation matrix of the parameters as a heat map.

Table 2
Statistical values of scaled experimental data.

Input and Output parameters	Min.	Max.	Avg.	Stand. Dev.
d/b	0	1	0.70	0.28
l/b	0	1	0.75	0.24
n	0	1	0.51	0.34
s/b	0	1	0.55	0.24
h	0	1	0.55	0.50
s_e/b	0	1	0.91	0.16
q_s/c_u	0	1	0.78	0.20

3.1. Data set normalization process

Normalizing datasets through scaling enhances prediction accuracy by mitigating the impact of bad data or missing values. In this study, the raw dataset was scaled to a range of 0 to 1 using a linear mapping function [26,27] based on equation 1.

$$\left(\frac{q_s}{c_u}\right)_n = \left[\frac{\left(\frac{q_s}{c_u}\right)_{high} - \left(\frac{q_s}{c_u}\right)}{\left(\frac{q_s}{c_u}\right)_{high} - \left(\frac{q_s}{c_u}\right)_{low}}\right] \quad (1)$$

where $\left(\frac{q_s}{c_u}\right)$ = data derived from the experimental dataset;

$\left(\frac{q_s}{c_u}\right)_n$ = scaled normalized output; and

$\left(\frac{q_s}{c_u}\right)_{high}$ & $\left(\frac{q_s}{c_u}\right)_{low}$ = highest and lowest unprocessed input values in the dataset, respectively. Table 1 presents the ranges of scaled input and output data derived from experimental studies, utilized in developing the ANN and M5P models.

4. Soft computing techniques

4.1. Artificial neural networks

An artificial neural network (ANN) is a computational model inspired by the way the human brain processes and analyzes information. ANN is widely used in geotechnical engineering for numerical predictions and resolving complex issues [18,28–31]. Inputs are fed into this model to predict micropile capacity. The neurons in the hidden layers process the datasets by applying weighted averages and algorithms to minimize errors. Once trained, the model is tested with new data to evaluate the accuracy of the predictions. After testing, the model can generate output even for unseen data. For multi-layer formation, the inputs are d/b, l/b, n, s/b, h, and s_e/b were used, with q_s/c_u as the output. A critical aspect of ANN is determining when to stop training. Training for too long can lead to overfitting (capturing noise), while stopping too early may result in poor prediction accuracy. Hence, the training iterations are carefully planned to achieve the best results. The mean square error and R^2 between the actual and predicted values were calculated for different iterations to evaluate the model's performance. During the training process, the default Sigmoid activation function was applied to calculate MSE and R^2 values for each epoch increment and as shown in Fig. 3. Based on Fig. 3, the number of epochs was set to 1,000 to achieve the lowest MSE and highest R^2. In ANNs, each neuron uses an activation function to calculate its output for a given input. These functions are essential for scaling outputs to appropriate ranges and introducing nonlinearity, which enhances the network's ability to address complex problems. Among the various activation functions, transfer functions are commonly preferred for their advantageous properties, including fast computation, bounded outputs, and their significance in approximation theory. This study employs different activation functions for the neurons in the hidden and output layers, including linear, sigmoid, sigmoid stepwise, gaussian, elliot, elliot symmetric, linear piece, linear piece symmetric, sin, sin symmetric, cos and cos symmetric functions. These activation functions are supported by the open-source Agiel neural network software [32]. The dataset, comprising 434 data points, was divided into two sets: 70% for training and 30% for testing as per [31,33,34].

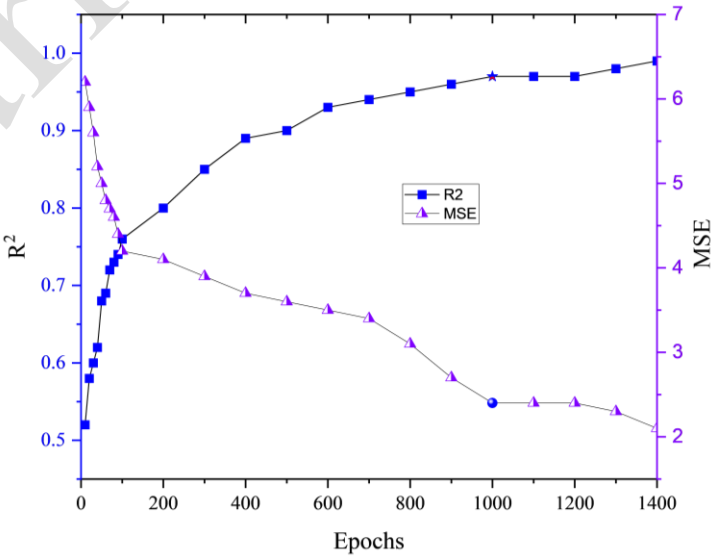

Fig. 3. Optimal epochs for ANN model.

The next step involves identifying the optimal number of neurons in the hidden layer. The model was run with varying numbers of neurons, and the corresponding Root Mean Square Error (RMSE) and R^2 values were calculated and presented in Figure 4. The optimal number of neurons (4) was determined based on the point where the R^2 value is closest to 1 and the RMSE is at its lowest [31,35,36].

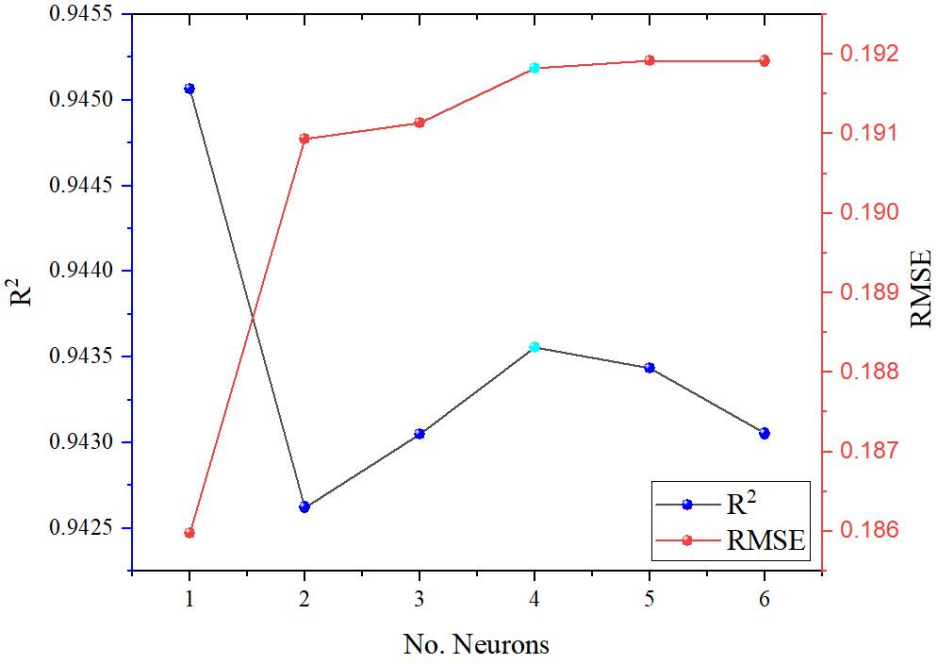

Fig. 4. Optimal hidden layer neuron count estimation.

Following these guidelines, the ANN model was designed with a single hidden layer containing four neurons, which proved sufficient for accurately predicting micro-pile group capacity (q_s/c_u). The final ANN structure (6 Input -4 Hidden-1 Output) is illustrated in Fig. 5.

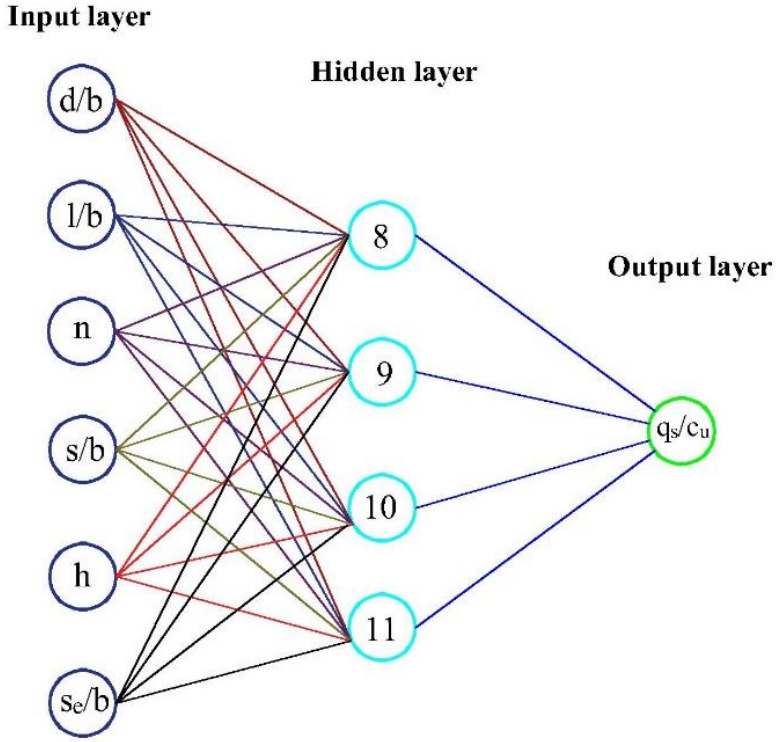

Fig. 5. Optimal structure of the ANNs model.

4.2. M5P-tree model (M5P)

The M5P-tree algorithm is designed to handle regression problems, which involve predicting numerical values [37]. The M5P algorithm creates a decision tree where each branch represents a decision based on an input feature, acting as an individual decision-maker. At the leaves (endpoints of the tree), the algorithm generates a linear regression equation for making predictions. The algorithm splits the tree into branches by dividing the data to minimize the prediction error. This process continues until the error is reduced to the lowest possible level. Initially, the tree may grow too complex, but the algorithm applies pruning to simplify the model by removing unnecessary branches, thereby preventing overfitting. The algorithm works like a decision tree, where each branch represents different parts of the data. At the endpoints of the branches, called leaves, linear regression models are applied to make predictions. The schematic architecture of the M5P model is shown in Fig. 6, 7 & 8. The M5P tree begins by dividing the input data into smaller groups, or subsets, based on shared features (Fig. 6).

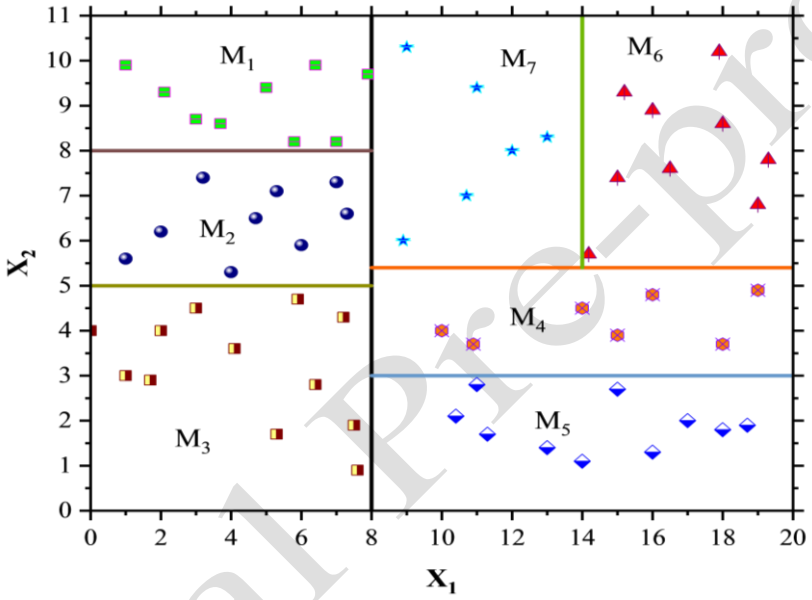

Fig. 6. M5P mode architecture.

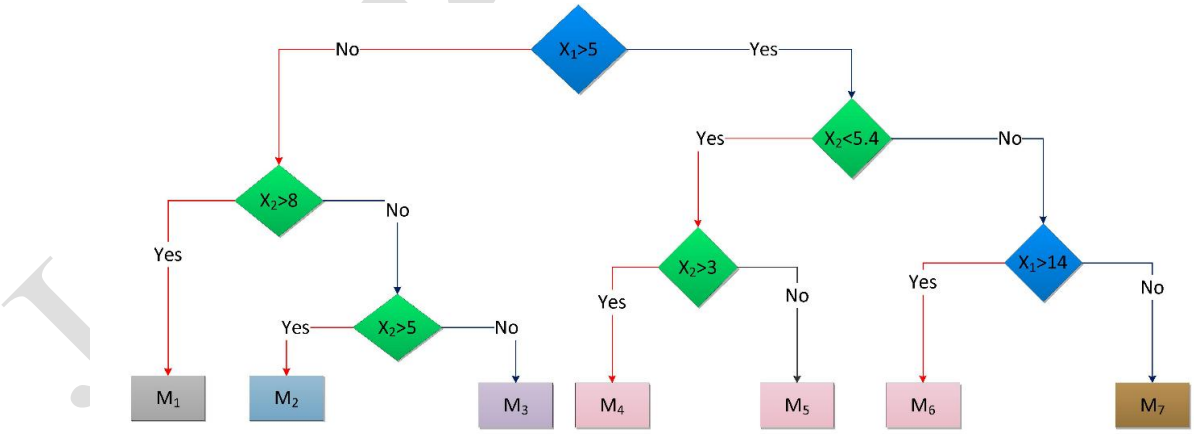

Fig. 7. The schematic view of the M5P model tree algorithm.

Within each subset, linear regression models may be used to address differences in the data. This process generates nodes, where each node splits the data according to a specific attribute (Fig. 7). The tree structure starts at the root (top), progresses through the nodes, and ends at the leaves (bottom). As new data is added, it flows through the tree, moving from root to leaf based on the splitting rules (Fig. 8).

To determine how to divide the data at each node, the algorithm calculates errors by deviation of the values of the group to the average of the group. It uses attributes that minimize this error to decide how to split the data and the error is calculated based on the standard deviation to know how values are spread-out. The splitting continues as long as the less errors are prevalent. To avoid complex issues of overfitting, where the model becomes too tailored to the training data, the algorithm applies a process called pruning. Pruning simplifies the tree by replacing overly complex branches with linear regression functions, making the model more general and effective for new data. The M5P-tree algorithm combines decision trees and linear regression to find numerical values. It splits data to minimize errors and prunes the tree to prevent overfitting, ensuring better performance on new datasets.

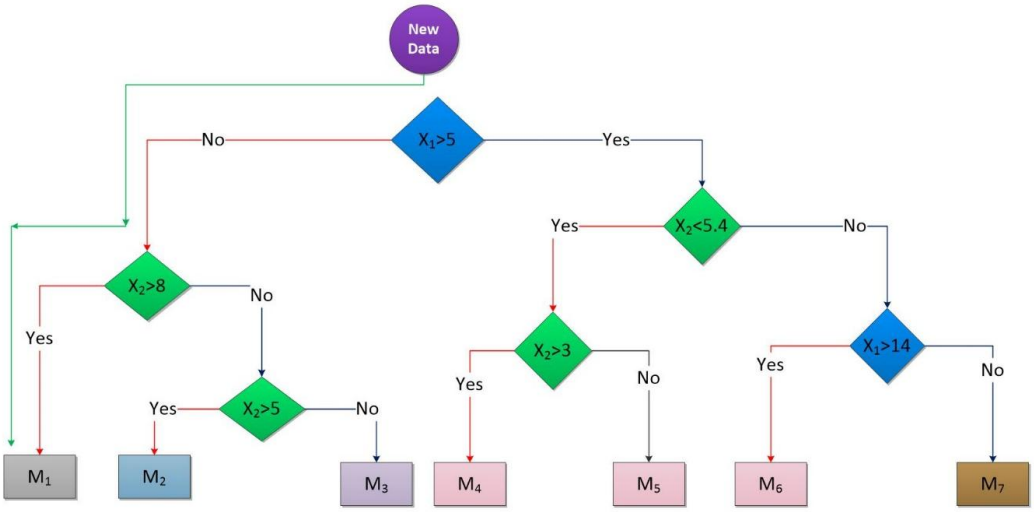

Fig. 8. The schematic view of the M5P model tree algorithm for new data.

Standard reduction using equation 2:

$$SDR = sd(T) - \sum \frac{|T_i|}{|T|} sd\left(T_i\right) \tag{2}$$

T - examples that reach a specific stage in the process

T_i - examples belonging to the i^{th} subset of a possible group

sd - standard deviation.

The multi-layer models used in this research were developed using Weka, a free and popular open-source software. Weka is widely used by engineers and scientists to analyze data and design systems that contribute to real-world advancements.

5. Model preparation

In this study, the modeling was performed using the open-source software AgieINN and WEKA for ANN and M5P modeling, respectively. It is important to note that WEKA incorporates k-fold cross-validation by randomly dividing the dataset into K subsamples, where one subsample is used for model testing and the remaining K-1 subsamples are used for training. This process is repeated K times, allowing each subsample to serve as testing data exactly once. In the present analysis, a 10-fold cross-validation (K=10) was employed within the WEKA environment to enhance model generalization and mitigate overfitting. The averaged results from the folds provide a more reliable performance estimate for the developed models. In

other hand, AgieINN is not having the provision to incorporate the k-fold cross-validation. Hence, the randomized data is directly fed to the software to do the training and testing. The hyperparameter parameters for the ANN and M5P model are shown in Table 3.

Table 3
Optimum values of hyperparameter parameters for ANN and M5P models.

Machine learning Model	Hyperparameter and user defined parameters
ANN	Learning rate = 0.7, momentum = 0.1, Iteration = 1000, Hidden layer = 1, Hidden layer neurons = 4
M5P	Minimum leaf size =4, Pruning factor =0.1

6. Performance measures

After identifying the model, its ability to predict the micro-pile group capacity must be evaluated using a test dataset. Since there is no universal agreement among researchers on the best metric for prediction accuracy, evaluating the model's performance requires minimizing errors. In this study, the metrics chosen for evaluation include mean absolute error (MAE), mean absolute percentage error (MAPE), mean square error (MSE), and root mean square error (RMSE). These metrics provide different insights into the model's performance:

MAE: This measures overall prediction accuracy by showing the average magnitude of errors without considering their direction. It treats all errors equally, making it zero for a perfect fit and higher for poor predictions. The method with the smallest MAE is preferred because it represents the most accurate predictions overall.

MSE: This also measures prediction accuracy but gives extra weight to larger errors by squaring them. While it indicates the spread of errors, it is more sensitive to significant deviations.

RMSE: As the square root of MSE, RMSE provides error measurements in the same unit as the predicted variable, making it easier to interpret. It shares MSE's sensitivity to large errors.

MAPE: This metric evaluates relative accuracy, making it useful for comparing predictions across different methods or datasets. It is expressed as a percentage and is unit-independent. MAPE interpretations include: < 10%: Excellent accuracy; between 10 and 20%: Good prediction; between 20 and 50%: Acceptable prediction; above 50%: Poor prediction.

In general, smaller values for MSE, RMSE, MAE, and MAPE indicate a better-performing model. However, each metric has its limitations. RMSE and MSE, for instance, are highly sensitive to outliers, which can distort the evaluation of accuracy. Some researchers suggest these metrics should be used cautiously. MAE, on the other hand, is considered more robust against outliers but may favor models that occasionally make large errors. When selecting a predictive model, the choice of error metric is critical as it influences the evaluation of prediction accuracy. While least-squares criteria are commonly used in estimation procedures, focusing solely on MAE might introduce inconsistencies. Additionally, relying only on traditional metrics such as the correlation coefficient (r) and the coefficient of determination (R^2) can lead to biased evaluations. Therefore, these should be complemented with unbiased statistical criteria like MSE, RMSE, MAE, and MAPE. Table 4 presents a detailed mathematical equation of the statistical parameters/error metrics/ performance measures used for evaluating the prediction of micropile group capacity. This comprehensive approach ensures that the selected model is robust and provides reliable predictions across various scenarios.

Table 4
Mathematical equations for performance measures.

Performance measures	Mathematical equation
Correlation coefficient (r)	$r=\frac{\sum\left(\frac{q_s}{c_u}\right)_{ht}\times\left(\frac{q_s}{c_u}\right)_{hp}-n\overline{\left(\frac{q_s}{c_u}\right)_{ht}}\times\overline{\left(\frac{q_s}{c_u}\right)_{hp}}}{(n-1)S_{\left(\frac{q_s}{c_u}\right)_{ht}}S_{\left(\frac{q_s}{c_u}\right)_{hp}}}$
Coefficient of determination (R^2)	$R^2=1-\frac{\sum_i\left(\left(\frac{q_s}{c_u}\right)_{hp}-\left(\frac{q_s}{c_u}\right)_{ht}\right)^2}{\sum_i\left(\left(\frac{q_s}{c_u}\right)_{hp}-\overline{\left(\frac{q_s}{c_u}\right)_{hp}}\right)^2}$
Mean square error (MSE)	$MSE=\frac{1}{n}\sum_{i=1}^{n}\left(\left(\frac{q_s}{c_u}\right)_{ht}-\left(\frac{q_s}{c_u}\right)_{hp}\right)^2$
Root mean square error (RMSE)	$RMSE=\sqrt{\frac{1}{n}\sum_{i=1}^{n}\left(\left(\frac{q_s}{c_u}\right)_{ht}-\left(\frac{q_s}{c_u}\right)_{hp}\right)^2}$
Mean absolute error (MAE)	$MAE=\frac{1}{n}\sum_{i=1}^{n}\left\lvert\left(\frac{q_s}{c_u}\right)_{ht}-\left(\frac{q_s}{c_u}\right)_{hp}\right\rvert$
Mean absolute percentage error (MAPE)	$MAPE=\left[\frac{1}{n}\sum_{i=1}^{n}\left\lvert\frac{\left(\frac{q_s}{c_u}\right)_{ht}-\left(\frac{q_s}{c_u}\right)_{hp}}{\left(\frac{q_s}{c_u}\right)_{ht}}\right\rvert\right]\times 100$

Note: $\left(\frac{q_s}{c_u}\right)_{ht}$, $\left(\frac{q_s}{c_u}\right)_{hp}$ target and predicted micro-pile group capacity respectively, $\overline{\left(\frac{q_s}{c_u}\right)_{ht}}$, $\overline{\left(\frac{q_s}{c_u}\right)_{hp}}$:mean of the target and predicted micro-pile group capacity respectively, $S_{\left(\frac{q_s}{c_u}\right)_{ht}}$, $S_{\left(\frac{q_s}{c_u}\right)_{hp}}$:standard deviation of the target and predicted micro-pile group capacity respectively, n: number of observations

7. Results, discussions and comparison

An ANN model with various activation functions was used to develop a prediction model for the capacity of micropile groups. The performance metrics of different activation functions are presented in Table 5.

Table 5
Performance measures for training, testing of ANN model.

Activation Function	Training						Testing					
	r	R^2	MSE	RMSE	MAE	MAPE	r	R^2	MSE	RMSE	MAE	MAPE
Cos	0.79	0.79	0.002	0.049	0.048	22.06	0.79	0.79	0.004	0.060	0.06	9.21
Cos symmetric	0.69	0.69	0.003	0.052	0.052	24.26	0.69	0.69	0.004	0.063	0.065	10.13
Elliot	0.59	0.59	0.003	0.055	0.056	27.57	0.59	0.59	0.005	0.067	0.07	11.51
Elliot symmetric	0.49	0.49	0.003	0.057	0.06	30.33	0.49	0.49	0.005	0.070	0.075	12.27
Gaussian	0.74	0.74	0.003	0.051	0.05	23.16	0.74	0.74	0.004	0.062	0.062	9.67
Linear	0.4	0.4	0.004	0.060	0.064	33.08	0.4	0.4	0.005	0.073	0.08	13.81
Linear Piece	0.64	0.64	0.003	0.053	0.054	25.73	0.64	0.64	0.004	0.065	0.067	10.75
Linear Piece symmetric	0.34	0.34	0.004	0.062	0.068	34.56	0.34	0.34	0.006	0.075	0.085	14.43
Sigmoid	**0.99**	**0.99**	**0.002**	**0.045**	**0.04**	**18.38**	**0.99**	**0.99**	**0.003**	**0.055**	**0.05**	**7.67**
Sigmoid stepwise	0.54	0.54	0.003	0.056	0.058	28.67	0.54	0.54	0.005	0.069	0.072	11.97
Sin	0.69	0.69	0.003	0.052	0.052	24.99	0.69	0.69	0.004	0.063	0.065	10.44
Sin symmetric	0.45	0.45	0.003	0.058	0.062	31.8	0.45	0.45	0.005	0.071	0.077	13.28

Bold indicates the best activation function

Based on Table 5, it can be concluded that the Sigmoid activation function model outperforms the other models. The Sigmoid model achieved an R^2 value close to 1 and low error metrics (MSE, RMSE, and MAPE), as shown in Table 5, indicating strong agreement between the predicted and measured values [31]. Graphs illustrating the relationship between predicted and measured values for training and testing are shown in Figures 9 and 10, respectively. These graphs demonstrate high correlation coefficients (r=0.99) for both training and testing, confirming the model's accuracy in predicting micropile group capacity. Further analysis of Figures 9 and 10 reveals that most data points fall within ±20% of the zero line. Additionally, a comparison of predicted and experimental values for testing data, shown in Figure 10, highlights that the ANN model predictions closely match the experimental results. Figure 9-11 further confirms the ANN model's precision in predicting micropile group capacity.

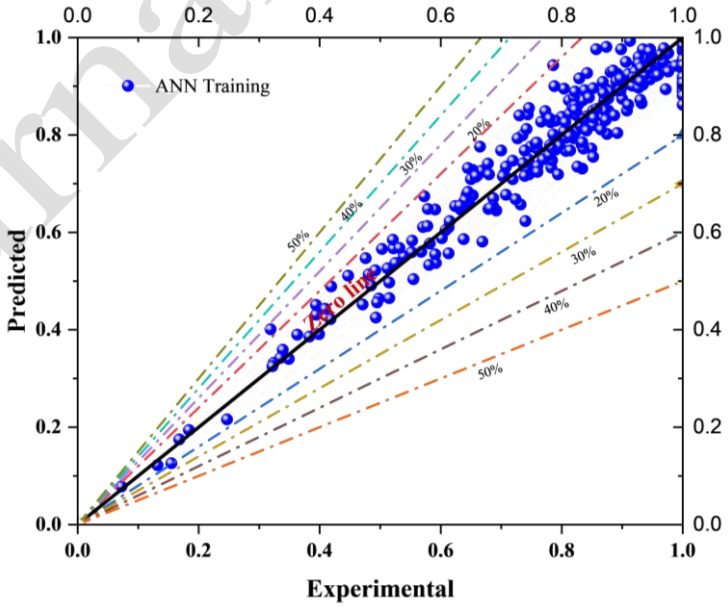

Fig. 9. Experimental Vs ANN predicted plot for training.

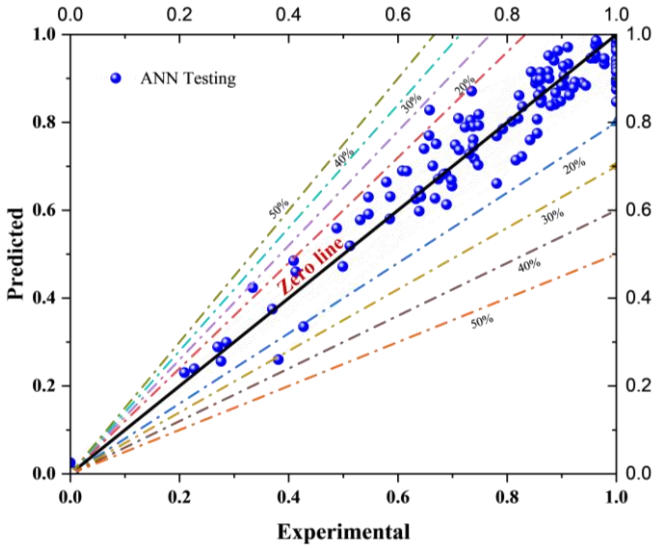

Fig. 10. Experimental Vs ANN predicted plot for testing.

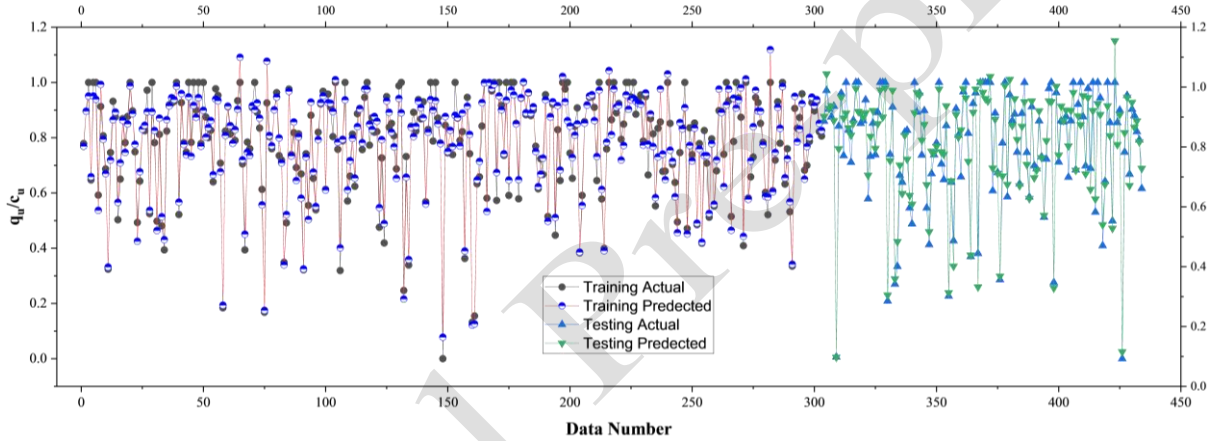

Fig. 11. ANN model comparison among the prediction and actual.

Similarly, an M5P model was developed using predefined parameters and validated using performance metrics. The results, summarized in Table 6, show low error values (MSE, RMSE, MAE, and MAPE) and an r value and R^2 close to 1, indicating good accuracy and correlation between predicted and target values.

Table 6
Performance measures for training and testing of M5P model.

Training						Testing					
r	R^2	MSE	RMSE	MAE	MAPE	r	R^2	MSE	RMSE	MAE	MAPE
0.99	0.99	0.00	0.06	0.05	23.92	0.99	0.99	0.00	0.06	0.05	10.01

Figures 12 and 13 present the predicted versus experimental results for training and testing, showing that most values lie within ±30% of the zero line. Finally, Figure 14 compares the experimental data with M5P-trained and M5P-tested predictions, demonstrating a close match between the experimental and M5P-predicted values, visually confirming the accuracy of the models. The performance measures indicate that the ANN model has lower error values compared to the M5P model. Therefore, the ANN model is more effective for predicting micro-pile group capacity.

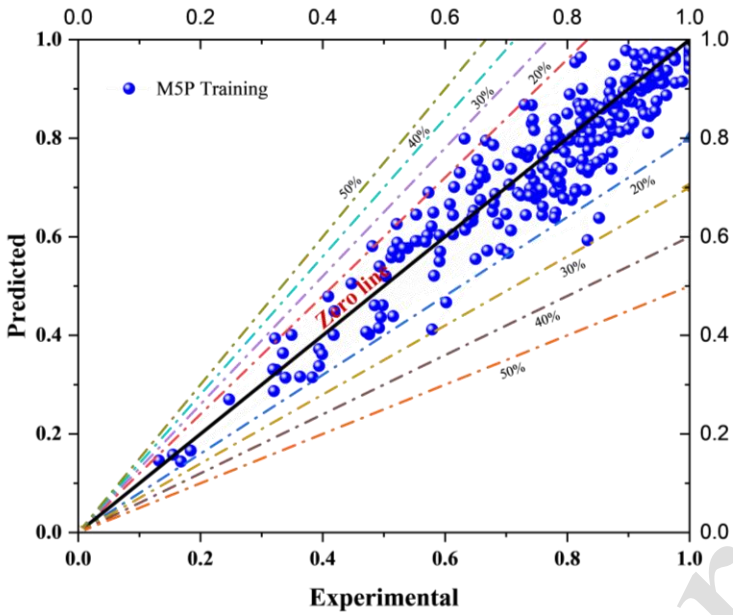

Fig. 12. M5P targeted Vs predicted plot for training.

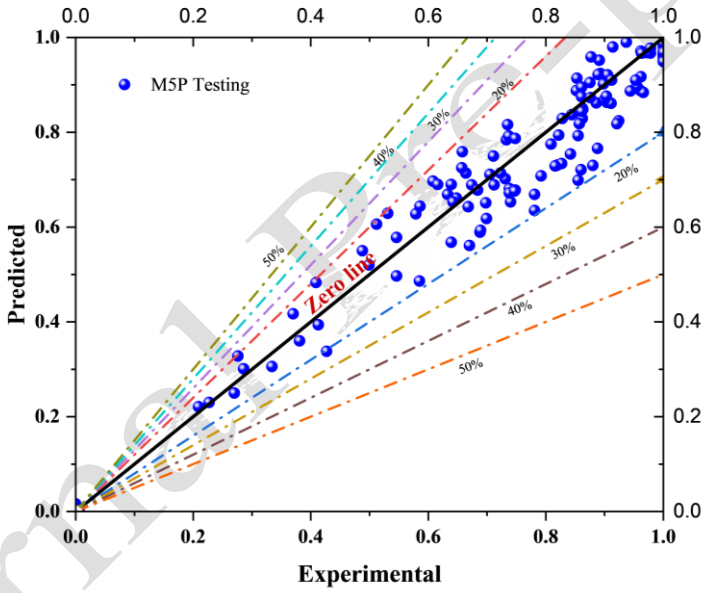

Fig. 13. M5P targeted Vs predicted plot for testing.

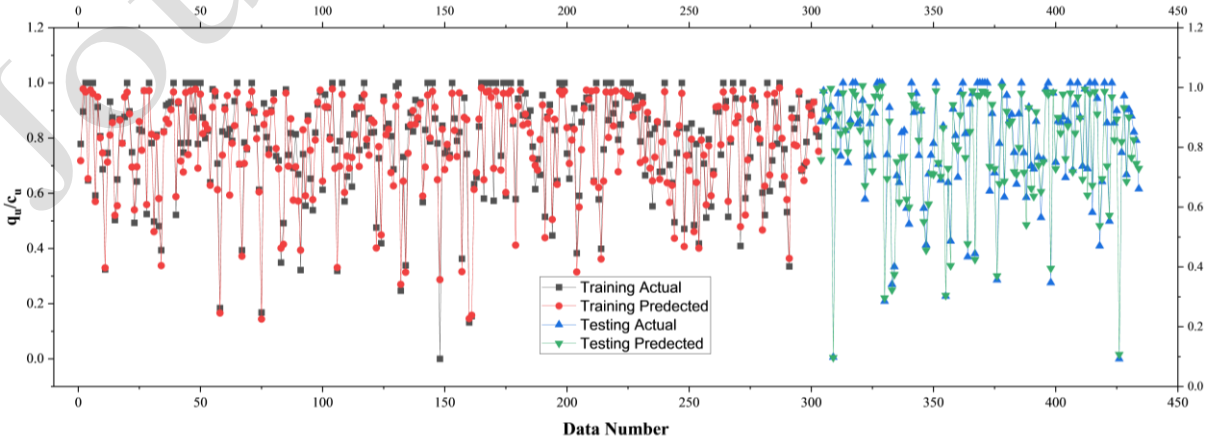

Fig. 14. M5P model comparison among the prediction and experimental.

Finally, The Taylor diagrams for both training (Fig. 15 (a)) and testing (Fig. 15 (b)) datasets reveal that the ANN and M5P models demonstrate strong predictive accuracy, as evidenced by high correlation coefficients in both phases. The ANN model consistently achieves a higher correlation (near 0.99) and lower standard deviation than the M5P model, indicating its greater predictive precision and reliability in both datasets. Overall, the ANN model aligns more closely with the reference dataset in both training and testing phases, highlighting its effectiveness in capturing the underlying data patterns.

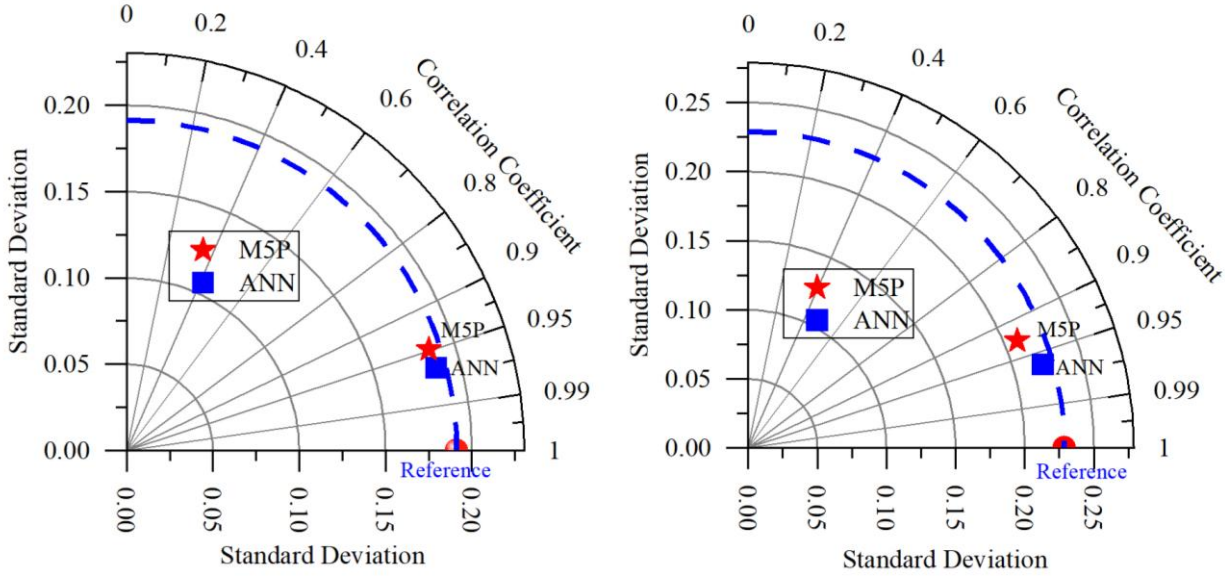

Fig. 15. Tylor's diagram for training (a) and testing (b).

It is pertinent to mention here that M5P decision tree structure, with linear regression equations at each leaf, effectively captures local linear relationships and approximates non-linear patterns piecewise, enhancing its predictive reliability. However, ANN excel in modeling complex, non-linear relationships through hidden layers and activation functions, making them more adept at handling intricate datasets. This difference demonstrates that ANN can outperform M5P in managing datasets with significant variability and complex patterns.

8. Model equation for ANN

Using the proposed 6-4-1 architecture shown in Fig. 5 and an optimal iteration count of 1000, the model was run to predict the micro-pile group capacity. The predictions were validated using performance measures. For the Sigmoid activation function, the weight matrices and biases were defined as follows: $[x_{ji}]$: Weights between the input layer's i^{th} neuron and the hidden layer's j^{th} neuron; $[y^{jk}]$: Weights between the hidden layer's jth neuron and the output layer's k^{th} neuron; $[z_j]$: Bias at the j^{th} neuron in the hidden layer; $[z_0]$: Bias at the output layer. These are detailed in Equations 3 to 6 and summarized in Table 7.

$$x_{ji} = \begin{bmatrix} x_{11} & x_{12} & x_{13} & x_{14} & x_{15} & x_{16} \\ x_{21} & x_{22} & x_{23} & x_{24} & x_{25} & x_{26} \\ x_{31} & x_{32} & x_{33} & x_{34} & x_{35} & x_{36} \\ x_{41} & x_{42} & x_{43} & x_{44} & x_{45} & x_{46} \end{bmatrix} = \begin{bmatrix} -0.30 & 1.81 & -8.89 & -1.94 & -3.60 & -5.34 \\ -0.63 & -4.86 & -1.45 & -1.45 & -2.06 & -4.59 \\ 1.95 & -1.05 & -1.08 & -0.88 & -0.91 & 0.05 \\ -0.80 & -1.52 & -4.98 & -2.83 & -2.89 & 6.50 \end{bmatrix} \quad (3)$$

$$y_{ji} = \begin{bmatrix} y_{11} \\ y_{21} \\ y_{31} \\ y_{41} \end{bmatrix} = \begin{bmatrix} 0.68 \\ 1.39 \\ -5.63 \\ -25.64 \end{bmatrix} \tag{4}$$

$$z_j = \begin{bmatrix} z_1 \\ z_2 \\ z_3 \\ z_4 \end{bmatrix} = \begin{bmatrix} -9.84 \\ 4.49 \\ 25.87 \\ -1.18 \end{bmatrix} \tag{5}$$

$$z_0 = \begin{bmatrix} -2.48 \end{bmatrix} \tag{6}$$

Further, the weights and biases as reported in Equations 3 to 6 were used to develop the ANN's model equation as followed by the basic Eq. 7 [38].

$$\left(\frac{q_s}{c_u}\right) = f_n\left\{z_0 + \sum_{j=1}^{h}\left[x_{jk} f_n\left(\sum_{i=1}^{n} y_{jk} X_i\right)\right]\right\} \tag{7}$$

Where,

h = number of neurons in hidden layer (4),

n = the number of neurons in input layer (6)

X_i = the normalized value of inputs.

The steps required to develop the model equation include the calculation of A1–A4 and b1–b4 using Equations 8 to 11 and Equations 12 to 15, respectively. The final expression takes the form as Equation 16. The be-normalized and the de-normalized forms of which are represented by Equations 17 and 18 respectively.

$$A_1 = x_{11} \times \frac{d}{b} + x_{12} \times \frac{l}{b} + x_{13} \times n + x_{14} \times \frac{s}{b} + x_{15} \times h + x_{16} \times \frac{s_e}{b} \tag{8}$$

$$A_2 = x_{21} \times \frac{d}{b} + x_{22} \times \frac{l}{b} + x_{23} \times n + x_{24} \times \frac{s}{b} + x_{25} \times h + x_{26} \times \frac{s_e}{b} \tag{9}$$

$$A_3 = x_{31} \times \frac{d}{b} + x_{32} \times \frac{l}{b} + x_{33} \times n + x_{34} \times \frac{s}{b} + x_{35} \times h + x_{36} \times \frac{s_e}{b} \tag{10}$$

$$A_4 = x_{41} \times \frac{d}{b} + x_{42} \times \frac{l}{b} + x_{43} \times n + x_{44} \times \frac{s}{b} + x_{45} \times h + x_{46} \times \frac{s_e}{b} \tag{11}$$

$$b_1 = \frac{1}{1 + e^{-A_1}} \tag{12}$$

$$b_2 = \frac{1}{1 + e^{-A_2}} \tag{13}$$

$$b_3 = \frac{1}{1+e^{-A_3}} \tag{14}$$

$$b_4 = \frac{1}{1+e^{-A_4}} \tag{15}$$

$$B_1 = b_1 + b_2 + b_3 + b_4 + z_0 \tag{16}$$

$$\left(\frac{q_s}{c_u}\right)_{be-normal} = \frac{1}{1+e^{-B_1}} \tag{17}$$

The $\left(\frac{q_s}{c_u}\right)$ value as obtained from Eq. (17) is in the range [-1, 1] and this needs to be denormalized as. The same procedure is proposed by [31,34].

$$\left(\frac{q_s}{c_u}\right)_{de-normal} = 0.5\left(\frac{q_s}{c_u}+1\right)\left(\left(\frac{q_s}{c_u}\right)_{\max} - \left(\frac{q_s}{c_u}\right)_{\min}\right) + \left(\frac{q_s}{c_u}\right)_{\min} \tag{18}$$

Where $\left(\frac{q_s}{c_u}\right)_{\max}$ and $\left(\frac{q_s}{c_u}\right)_{\min}$ are the maximum and minimum values of $\left(\frac{q_s}{c_u}\right)$ respectively in the data set.

Table 7
ANN model connection weights and biases.

Hidden neurons	Weights							Bias	
	d/b	*l/b*	*n*	*s/b*	*h*	s_e/b	q_s/c_u		
7	-0.30	1.81	-8.89	-1.94	-3.60	-5.34	0.68	-9.84	-2.48
8	-0.63	-4.86	-1.45	-1.45	-2.06	-4.59	1.39	4.49	
9	1.95	-1.05	-1.08	-0.88	-0.91	0.05	-5.63	25.87	
10	-0.80	-1.52	-4.98	-2.83	-2.89	6.50	-25.64	-1.18	

The calculation procedure for the proposed ANN model equation to determine the micro-pile group capacity is provided as a numerical example at the end of the article, before the references.

9. Model equation for M5P

The training and testing method is a common approach for developing learning algorithms and building models. In this process, the dataset is processed through two categories in which 70% for training the model, and the remaining 30% is used for testing and evaluating its performance. Table 1 depicts the standard deviation, minimum and maximum values of the parameters used to create the M5P model. The linear models developed using the M5P technique is expressed by the following Equations 19–23 and are presented in Figure 16. The equations should be applied according to the conditions indicated in Figure 16, which are labeled as M1 to M5.

$$\left(\frac{q_s}{c_u}\right)_1 = 0.24\times\frac{l}{b} + 0.02\times n + 0.03\times\frac{s}{b} + 0.19\times\frac{s_e}{b} + 0.19 \tag{19}$$

$$\left(\frac{q_s}{c_u}\right)_2 = 0.09\times\frac{l}{b} + 0.02\times n + 0.03\times\frac{s}{b} + 0.19\times\frac{s_e}{b} + 0.41 \tag{20}$$

$$\left(\frac{q_s}{c_u}\right)_3 = 1.0\times\frac{d}{b} + 0.13\times\frac{l}{b} + 0.13\times n + 0.05\times\frac{s}{b} + 0.37\times\frac{s_e}{b} - 0.67 \tag{21}$$

$$\left(\frac{q_s}{c_u}\right)_4 = 0.007\times\frac{d}{b} + 0.23\times\frac{l}{b} + 0.10\times n + 0.16\times\frac{s}{b} + 0.002\times h + 8.28\times\frac{s_e}{b} - 7.69 \tag{22}$$

$$\left(\frac{q_s}{c_u}\right)_5 = 0.01\times\frac{d}{b} + 0.05\times\frac{l}{b} + 0.03\times n + 0.04\times\frac{s}{b} - 0.004\times h + 2.64\times\frac{s_e}{b} - 1.75 \tag{23}$$

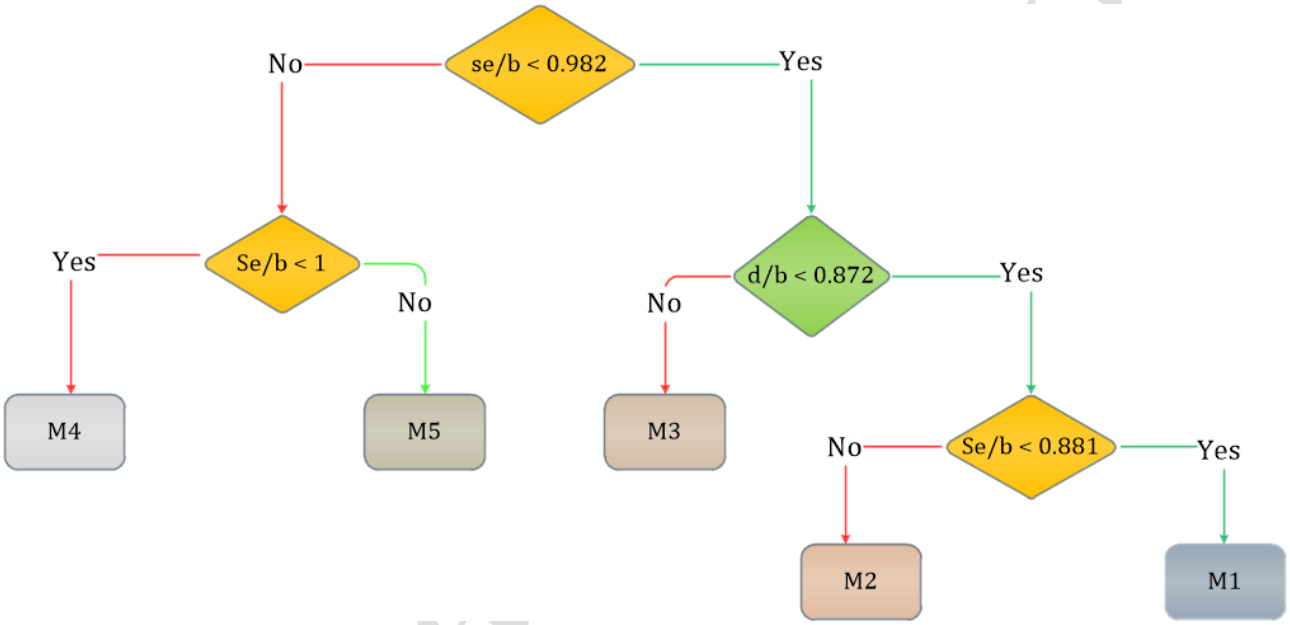

Fig. 16. Proposed M5P model tree to forecast the compressive strength of concrete.

10. Sensitivity analysis

This section of the study analyzes how individual variables affect the capacity of micro-pile groups using sensitivity analysis. Two methods, proposed by Garson [39] & Olden and Jackson [40] , were applied. In Garson [39], the connection weights of each hidden neuron in the hidden layer are divided into components, as demonstrated in the work of [41]. However, the method proposed by Garson [39] [40] has limitations, as it only considers the absolute values of the weights. These components, associated with each input variable, are listed in Table 5 along with the weights and biases. In the method by Olden and Jackson [40], the contribution of each input variable is calculated as the sum of the products of the final weights connecting input neurons to hidden neurons and then to the output. The results are obtained by following the procedures outlined in their studies. The findings, shown in Fig. 17, indicate that according to [40], the most influential parameter is *n*, followed by S_e/b, *s/b*, *h*, *l/b*, and *d/b*. [40] identifies S_e/b as the most significant factor, particularly due to its impact on erodible soils under rainfall, followed by *n* and *s/b*. Both methods showed marginal differences in their results, with the top two influencing parameters being consistent across the approaches. Therefore, it can be concluded that the identification of significant input parameters using Garson's [40] algorithm and the connection weight Olden and Jackson approach [40]

aligns well with the physical interpretation of capacity of micro-pile groups. This similar approach was flowed by [35,36]

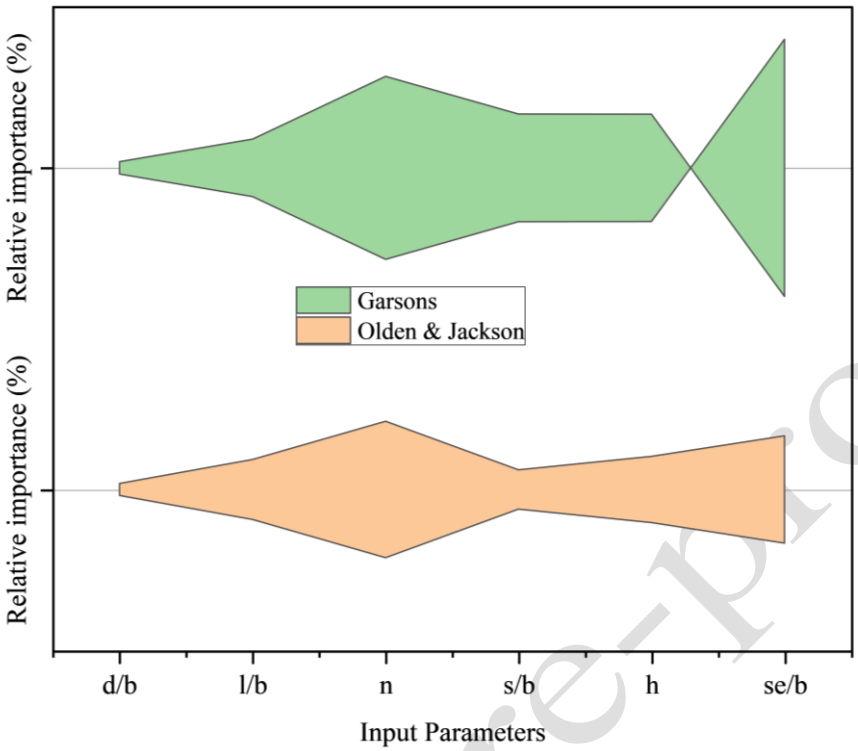

Fig. 17. Relative importance (%) of individual input variables on the micro-pile group capacity.

11. Conclusions

This article examines the applicability of Artificial Neural Networks (ANN) and M5P models for evaluating the load-carrying capacity of micropile groups in soft to very soft clayey soils, considering various input variables. The data used to develop and validate the ANN and M5P models were sourced from literature, specifically from experimental tests conducted on square micropile groups subjected to vertical load in a test pit. The following conclusions were drawn based on the findings from both the ANN and M5P models regarding the load capacity of the micropile groups:

- The accuracy, expressed in terms of the mean absolute percentage error (MAPE), was determined to be approximately ±20% for the ANN model and ±30% for the M5P model. The errors observed in the ANN model were lower compared to those in the M5P model, indicating that ANN predictions were more accurate for determining micropile group load capacity.
- 70% of the dataset was used for training the models, while the remaining 30% was reserved for testing in both models.
- In the sensitivity analysis, the parameter Se/b was found to play a vital role in the predictions, followed closely by n.

To broaden the research, future work could explore a wider range of machine learning algorithms, including Random Forest, XGBoost, CatBoost, Support Vector Regression (SVR), and Particle Swarm Optimization (PSO), to offer a more thorough evaluation of their performance relative to the current models. Additionally, integrating original field or experimental data, instead of depending entirely on existing datasets, would strengthen the study's novelty and reliability.

12. Example

Calculation Procedure of Micro-pile Group Capacity for the Developed ANN Model

Table. ex1
Sample dataset.

d/b	l/b	n	s/b	h	s_e/b	q_s/c_u
0.8	0.769	0.467	0.475	1	0.916	0.503

$$A_1 = x_{11} \times \frac{d}{b} + x_{12} \times \frac{l}{b} + x_{13} \times n + x_{14} \times \frac{s}{b} + x_{15} \times h + x_{16} \times \frac{s_e}{b} \quad (8)$$

A1= -12.41268

$$A_2 = x_{21} \times \frac{d}{b} + x_{22} \times \frac{l}{b} + x_{23} \times n + x_{24} \times \frac{s}{b} + x_{25} \times h + x_{26} \times \frac{s_e}{b} \quad (9)$$

A_2=-11.87168

$$A_3 = x_{31} \times \frac{d}{b} + x_{32} \times \frac{l}{b} + x_{33} \times n + x_{34} \times \frac{s}{b} + x_{35} \times h + x_{36} \times \frac{s_e}{b} \quad (10)$$

A_3=-1.03401

$$A_4 = x_{41} \times \frac{d}{b} + x_{42} \times \frac{l}{b} + x_{43} \times n + x_{44} \times \frac{s}{b} + x_{45} \times h + x_{46} \times \frac{s_e}{b} \quad (11)$$

A_4=-2.41479

Where the x coefficient values for the Eq. 7,8,9,10 can be read from the matrix Eq. 2

$$b_1 = \frac{1}{1+e^{-A_1}} \quad (12)$$

b_1=4.06668E-06

$$b_2 = \frac{1}{1+e^{-A_2}} \quad (13)$$

b_2=6.98541E-06

$$b_3 = \frac{1}{1+e^{-A_3}} \quad (14)$$

b_3=0.262307421

$$b_4 = \frac{1}{1+e^{-A_4}} \quad (15)$$

b_4=0.082051816

$$B_1 = b_1 + b_2 + b_3 + b_4 + z_0 \quad (16)$$

Where Z_0 is from Eq. 5

B_1=-2.135629711

$$\left(\frac{q_s}{c_u}\right)_{be-normal} = \frac{1}{1+e^{-B_1}} \tag{17}$$

$$\left(\frac{q_s}{c_u}\right)_{be-normal} = 0.105681728$$

$$\left(\frac{q_s}{c_u}\right)_{de-normal} = 0.5\left(\frac{q_s}{c_u}+1\right)\left(\left(\frac{q_s}{c_u}\right)_{\max} - \left(\frac{q_s}{c_u}\right)_{\min}\right) + \left(\frac{q_s}{c_u}\right)_{\min} \tag{18}$$

$$\left(\frac{q_s}{c_u}\right)_{de-normal} = 0.5\left(0.105681728+1\right)\left(1-0\right)+0$$

$$\left(\frac{q_s}{c_u}\right)_{de-normal} = 0.552840864$$

CRediT authorship contribution statement

Tammineni Gnananandarao: Conceptualization, Data curation, Formal analysis, Investigation, Methodology, Project administration, Resources, Software, Supervision, Writing – original draft, Writing – review & editing.

Naga Dheeraj Kumar Reddy Chukka: Conceptualization, Data curation, Methodology, Software, Supervision, Writing – original draft.

B.A.V. Ram Kumar: Data curation, Methodology, Validation, Writing – review & editing.

Jayatheja Muktinutalapati: Formal analysis, Validation, Writing – review & editing.

Vedprakash Maralapalle: Formal analysis, Validation, Writing – review & editing.

Satish Kumar Mummidivarapu: Investigation, Project administration, Visualization, Validation, Writing – review & editing.

CH. Ajay: Investigation, Project administration, Visualization, Writing – review & editing.

P. Uma Maheswara Rao: Investigation, Project administration, Visualization, Writing – review & editing.

References

[1] PJ S, T A, P G, Keeley J, B. T. Micropile Design and Construction. https://rosap.ntl.bts.gov/view/dot/50231. Fed Highw Adm Washingt 2025.

[2] Tsukada Y, Ichimura Y. Micropiles in Japan: Present status and future prospects. Int. Workshop on Micropiles. Seattle, Japan 1997.

[3] Bruce DA, DiMillio AF, Juran I. Micropiles: the state of practice Part 1: Characteristics, definitions and classifications. Proc Inst Civ Eng - Gr Improv 1997;1:25–35. https://doi.org/10.1680/gi.1997.010104.

[4] Borthakur N, Dey AK. Experimental Investigation on Load Carrying Capacity of Micropiles in Soft Clay. Arab J Sci Eng 2018;43:1969–81. https://doi.org/10.1007/s13369-017-2894-3.

[5] Han J, Ye S-L. A field study on the behavior of micropiles in clay under compression or tension. Can Geotech J 2006;43:19–29. https://doi.org/10.1139/t05-089.

[6] Kershaw KA, Luna R. Full-Scale Field Testing of Micropiles in Stiff Clay Subjected to Combined Axial and Lateral Loads. J Geotech Geoenvironmental Eng 2014;140:255–61. https://doi.org/10.1061/(ASCE)GT.1943-5606.0000968.

[7] Abd Elaziz AY, El Naggar MH. Group behaviour of hollow-bar micropiles in cohesive soils. Can Geotech J 2014;51:1139–50. https://doi.org/10.1139/cgj-2013-0409.

[8] Fayyad U, Piatetsky-Shapiro G, Smyth P. The KDD process for extracting useful knowledge from volumes of data. Commun ACM 1996;39:27–34. https://doi.org/10.1145/240455.240464.

[9] Shahin MA, Jaksa MB, Maier HR. Artificial neural network applications in geotechnical engineering. Aust Geomech 2001;36:49–62.

[10] Barkhordari MS, Fattahi H, Armaghani DJ, Khan NM, Afrazi M, Asteris PG. Failure mode identification in reinforced concrete flat slabs using advanced ensemble neural networks. Multiscale Multidiscip Model Exp Des 2024;7:5759–73. https://doi.org/10.1007/s41939-024-00554-9.

[11] Lee S., Lee S., Kim Y. An approach to estimate unsaturated shear strength using artificial neural network and hyperbolic formulation. Comput Geotech 2003;30:489–503. https://doi.org/10.1016/S0266-352X(03)00058-2.

[12] Zhang C, Zhu Z, Liu F, Yang Y, Wan Y, Huo W, et al. Efficient machine learning method for evaluating compressive strength of cement stabilized soft soil. Constr Build Mater 2023;392:131887. https://doi.org/10.1016/j.conbuildmat.2023.131887.

[13] Gnananandarao T, Dutta RK, Khatri VN, Kumar MS. Soft computing based prediction of unconfined compressive strength of fly ash stabilised organic clay. J Soft Comput Civ Eng 2022;6:43–58.

[14] Onyelowe KC, Gnananandarao T, Ebid AM. Estimation of the erodibility of treated unsaturated lateritic soil using support vector machine-polynomial and -radial basis function and random forest regression techniques. Clean Mater 2022;3:100039. https://doi.org/10.1016/j.clema.2021.100039.

[15] Noorzaei J, Hakim SJS, Jaafar MS. An approach to predict ultimate bearing capacity of surface footings using artificial neural network. Indian Geotech J 2008;38:515–28.

[16] Dutta RK, Gnananandarao T, Khatri VN. Application of soft computing techniques in predicting the ultimate bearing capacity of strip footing subjected to eccentric inclined load and resting on sand. J Soft Comput Civ Eng 2019;3:30–42.

[17] Gnananandarao T, Kumar Dutta R, Khatri VN. Tsunamigenic Seismic Activity (Earthquakes) Prediction from III- Component Seismic Data, 2021, p. 351–60. https://doi.org/10.1007/978-981-15-9976-7_31.

[18] Kohestani VR, Hassanlourad M, BAZARGAN LMR. Prediction the ultimate bearing capacity of shallow foundations on the cohesionless soils using M5P model tree 2016.

[19] López Paredes CR, García C, Onyelowe KC, Zuniga Rodriguez MG, Gnananandarao T, Andrade Valle AI, et al. Evaluating the impact of industrial wastes on the compressive strength of concrete using closed-form machine learning algorithms. Front Built Environ 2024;10. https://doi.org/10.3389/fbuil.2024.1453451.

[20] Gnananandarao T, Naik S V, Onyelowe KC, Panwar V. Forecasting Bearing Capacity, Error Analyses and Parametric Analysis of Circular Footing Seating on the Limited Thick Sand-Layer with Eccentric-Inclined Load. Civ Eng Infrastructures J 2025;58:87–102.

[21] Borthakur N, Dey AK. Evaluation of group capacity of micropile in soft clayey soil from experimental analysis using SVM-based prediction model. Int J Geomech 2020;20:4020008. https://doi.org/0.1061/%28ASCE%29GM.1943-5622.0001.

[22] Armaghani DJ, Liu Z, Khabbaz H, Fattahi H, Li D, Afrazi M. Tree-Based Solution Frameworks for Predicting Tunnel Boring Machine Performance Using Rock Mass and Material Properties. Comput Model Eng Sci 2024;141:2421–51. https://doi.org/10.32604/cmes.2024.052210.

[23] Yang B, Jahed Armaghani D, Fattahi H, Afrazi M, Koopialipoor M, Asteris PG, et al. Optimized Random Forest Models for Rock Mass Classification in Tunnel Construction. Geosciences 2025;15:47. https://doi.org/10.3390/geosciences15020047.

[24] Huat CY, Moosavi SMH, Mohammed AS, Armaghani DJ, Ulrikh DV, Monjezi M, et al. Factors Influencing Pile Friction Bearing Capacity: Proposing a Novel Procedure Based on Gradient Boosted Tree Technique. Sustainability 2021;13:11862. https://doi.org/10.3390/su132111862.

[25] Jahed Armaghani D, Hayati M, Momeni E, Dowlatshahi MB, Asteris PG. Estimation of powder factor in mine blasting: feasibility of tree-based predictive models. Multiscale Multidiscip Model Exp Des 2025;8:138. https://doi.org/10.1007/s41939-024-00725-8.

[26] Guide MU. Neural network toolbox. The MathWorks 2002;40.

[27] Ince R. Prediction of fracture parameters of concrete by Artificial Neural Networks. Eng Fract Mech 2004;71:2143–59. https://doi.org/10.1016/j.engfracmech.2003.12.004.

[28] Dutta RK, Rani R, Gnananandarao T. Prediction of ultimate bearing capacity of skirted footing resting on sand using artificial neural networks. J Soft Comput Civ Eng 2018;2:34–46.

[29] Acharyya R, Dey A, Kumar B. Finite element and ANN-based prediction of bearing capacity of square footing resting on the crest of c - φ soil slope. Int J Geotech Eng 2020;14:176–87. https://doi.org/10.1080/19386362.2018.1435022.

[30] Acharyya R, Dey A. Assessment of bearing capacity for strip footing located near sloping surface considering ANN model. Neural Comput Appl 2019;31:8087–100. https://doi.org/10.1007/s00521-018-3661-4.

[31] Dutta RK, Dutta K, Jeevanandham S. Prediction of Deviator Stress of Sand Reinforced with Waste Plastic Strips Using Neural Network. Int J Geosynth Gr Eng 2015;1:11. https://doi.org/10.1007/s40891-015-0013-7.

[32] Onyelowe KC, Kamchoom V, Gnananandarao T, Arunachalam KP. Developing data driven framework to model earthquake induced liquefaction potential of granular terrain by machine learning classification models. Sci Rep 2025;15:21509. https://doi.org/10.1038/s41598-025-07494-5.

[33] Panwar V, Dutta RK. Bearing capacity of rectangular footing on layered sand under inclined loading. J Achiev Mater Manuf Eng 2021;108:49–62. https://doi.org/10.5604/01.3001.0015.5064.

[34] Das SK, Basudhar PK. Undrained lateral load capacity of piles in clay using artificial neural network. Comput Geotech 2006;33:454–9. https://doi.org/10.1016/j.compgeo.2006.08.006.

[35] Ferreira FPV, Shamass R, Limbachiya V, Tsavdaridis KD, Martins CH. Lateral–torsional buckling resistance prediction model for steel cellular beams generated by Artificial Neural Networks (ANN). Thin-Walled Struct 2022;170:108592. https://doi.org/10.1016/j.tws.2021.108592.

[36] Panwar V, Dutta RK. Application of machine learning technique in predicting the bearing capacity of rectangular footing on layered sand under inclined loading. J Soft Comput Civ Eng 2022;6:130–52.

[37] Quinlan JR. Learning with continuous classes. 5th Aust. Jt. Conf. Artif. Intell., vol. 92, World Scientific; 1992, p. 343–8.

[38] Goh ATC, Kulhawy FH, Chua CG. Bayesian Neural Network Analysis of Undrained Side Resistance of Drilled Shafts. J Geotech Geoenvironmental Eng 2005;131:84–93. https://doi.org/10.1061/(ASCE)1090-0241(2005)131:1(84).

[39] Garson DG. Interpreting neural network connection weights 1991.

[40] Olden JD, Jackson DA. Illuminating the “black box”: a randomization approach for understanding variable contributions in artificial neural networks. Ecol Modell 2002;154:135–50. https://doi.org/10.1016/S0304-3800(02)00064-9.

[41] Onyelowe KC, Gnananandarao T, Nwa-David C. Sensitivity analysis and prediction of erodibility of treated unsaturated soil modified with nanostructured fines of quarry dust using novel artificial neural network. Nanotechnol Environ Eng 2021;6:37. https://doi.org/10.1007/s41204-021-00131-2.